

225 (1972); R. F. Casten, P. W. Keaton, Jr., and P. G. Lawrence, *Phys. Rev. C* **7**, 1016 (1973); R. D. Rathmell, P. J. Bjorkholm, and W. Haeberli, *Nucl. Phys. A206*, 459 (1973); J. A. Aymar, H. R. Hiddleston, S. E. Darden, and A. A. Rollefson, *Nucl. Phys. A207*, 596 (1973).

<sup>4</sup>S. E. Vigdor, R. D. Rathmell, H. S. Liers, and W. Haeberli, *Nucl. Phys. A210*, 70 (1973).

<sup>5</sup>H. S. Liers, R. D. Rathmell, S. E. Vigdor, and W. Haeberli, *Phys. Rev. Lett.* **26**, 261 (1971).

<sup>6</sup>G. Spaelek *et al.*, in *Polarization Phenomena in Nuclear Reactions*, edited by H. H. Barschall and W. Haeberli (Univ. of Wisconsin Press, Madison, Wis., 1971), p. 749; D. Hilsher, P. A. Quin, and J. C. Davis, *ibid.*, p. 752; J. Taylor *et al.*, *ibid.*, p. 754.

<sup>7</sup>Ch. Leemann, H. E. Conzett, W. Dahme, J. Macdonald, and J. P. Meulders, *Bull. Amer. Phys. Soc.* **17**, 562 (1972), and to be published.

<sup>8</sup>W. C. Parkinson *et al.*, *Phys. Rev.* **178**, 1976 (1969).

<sup>9</sup>F. D. Becchetti, Jr., and G. W. Greenlees, in *Polarization Phenomena in Nuclear Reactions*, edited by H. H. Barschall and W. Haeberli (Univ. of Wisconsin Press, Madison, Wis., 1971), p. 682.

<sup>10</sup>J. Testoni, private communication.

### Further Observation of Muonless Neutrino-Induced Inelastic Interactions\*

B. Aubert,<sup>†</sup> A. Benvenuti, D. Cline, W. T. Ford, R. Imlay, T. Y. Ling, A. K. Mann, F. Messing, R. L. Piccioni,<sup>‡</sup> J. Pilcher,<sup>§</sup> D. D. Reeder, C. Rubbia, R. Stefanski, and L. Sulak  
*Department of Physics, Harvard University, Cambridge, Massachusetts 02138, and*  
*Department of Physics, University of Pennsylvania, Philadelphia, Pennsylvania 19104, and*  
*Department of Physics, University of Wisconsin, Madison, Wisconsin 53706, and*  
*National Accelerator Laboratory, Batavia, Illinois 60510*  
 (Received 19 March 1974)

We report here additional positive results of a search for muonless neutrino- and antineutrino-induced events using an enriched antineutrino beam and a muon identifier of relatively high geometric detection efficiency. The ratio of muonless to muon event rates is observed to be  $R = 0.20 \pm 0.05$ . We observe no background derived from ordinary neutrino or antineutrino interactions that is capable of explaining the muonless signal.

The investigation reported here is a search for inelastic neutrino and antineutrino interactions at a mean energy of 40 GeV that differ from the usual processes by the absence of a muon in the final state.<sup>1</sup> A previous search for such events yielded a positive signal. Muonless events have also been reported in a CERN-Gargamelle experiment at a mean energy in the range of 2 to 4 GeV.<sup>2</sup>

The experiment was carried out at the National Accelerator Laboratory, where collisions of 300-GeV protons with an aluminum target produced secondary hadrons that were focused by a single magnetic horn to provide a beam enriched in antineutrinos.<sup>3</sup> The experimental apparatus [Fig. 1(a)] is a modified version of the arrangement described previously.<sup>1,4</sup> The modifications are (1) the addition of 35 cm of iron immediately downstream of the ionization calorimeter to form a muon identifier ( $\mu_1$ ) consisting of counter *B* and spark chamber 4, and (2) doubling of the area of counter *C* and replacement of the 5.3-m<sup>2</sup> narrow-gap spark chambers in the magnetic spectrometer with 8.4-m<sup>2</sup> wide-gap chambers to increase the solid angle of the second (original) muon

identifier ( $\mu_2$ ).

The experiment was triggered by the deposition of energy (*E*) in the ionization calorimeter greater than a preset minimum value,<sup>5</sup> with counter *A* in anticoincidence. The hadron cascade of an actual event is illustrated in Fig. 1(b) and the track pattern observed in spark chambers SC1-SC8 is illustrated in Fig. 1(c) which shows one of the three stereoscopic views of the event. Events were verticized by extrapolation of tracks in the two  $\pm 7.5^\circ$  stereo views and in the  $90^\circ$  stereo view, and consistency was required between the *z* position obtained from the visual reconstruction of the vertex and the calorimeter pulse-height information.

The *z* dependence of all triggers was observed to be uniform except for a small excess of events in the first segment (module) of the target detector, which is consistent with the small (5%) geometrical inefficiency of counter *A*. There is no evidence of neutrons or photons, unaccompanied by charged particles, entering the front of the target. Since each segment of the calorimeter corresponds to approximately 0.6 nuclear collision lengths, to provide additional protection

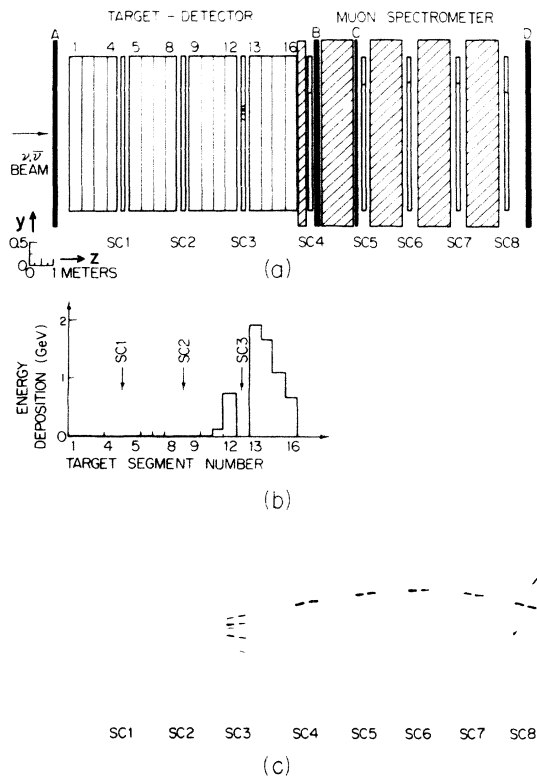


FIG. 1. (a) Plan view of the modified experimental apparatus. The target detector consists of liquid scintillator segments (1-16) with wide-gap spark chambers (SC1-SC4) interspersed. The muon spectrometer includes SC5-SC8. Auxiliary scintillation counters are A, B, C, and D. An inelastic neutrino event with an associated muon is sketched into the spark chambers (c) and the energy deposition in each segment is shown in (b).

from penetrating hadrons, events occurring upstream of module 5 were excluded. A further restriction,  $z \leq 12$ , was imposed to reserve 4 modules for detection of the hadronic cascade and as additional absorber for  $\mu_1$ .

Events can be tentatively classified as having a muon or not according to the response of scintillation counter B, and are labeled  $\bar{A}EB$  and  $\bar{A}E\bar{B}$ , respectively. In Fig. 2 are shown the distributions in hadron energy,  $E_H$ , for the 1410 triggers in the  $z$  fiducial region. The shaded histograms show those events for which a hadron shower with a reconstructed vertex was present in the spark chambers. Except for very low-energy  $\bar{A}E\bar{B}$  triggers, about two-thirds of the events have a reconstructed vertex.<sup>6</sup> The remainder can be accounted for in the main by neutrino interactions in the calorimeter beyond the spark

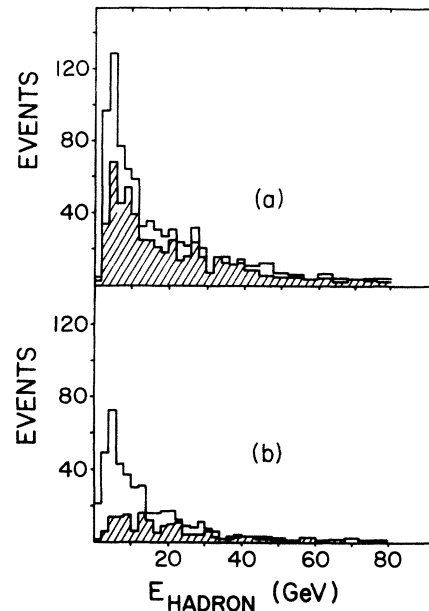


FIG. 2. (a) The  $E_H$  distribution of all  $\bar{A}EB$  triggers (951) and of the corresponding verticized events (627, cross-hatched). (b) The  $E_H$  distribution of all  $\bar{A}E\bar{B}$  triggers (459) and the corresponding verticized events (173, cross-hatched).

chamber boundaries. The larger excess of low-energy  $\bar{A}E\bar{B}$  triggers appears to be diffuse showers that originate outside the target, of which only traces are seen in the spark chambers.

The distribution of shower vertices in the transverse plane is nearly uniform, with a small depletion toward the target boundary consistent with the neutrino beam rms radius of  $\sim 1.5$  m. A fiducial boundary limit of  $\pm 120$  cm in  $x$  and  $y$  was imposed to avoid regions of low detection efficiency and to insure complete rejection of hadrons entering the sides.<sup>7</sup> A total of 535 events passed the threshold on  $E_H$  and satisfied the criteria on vertex location, event quality, and time of occurrence within the beam gate.

To use counter B or SC4 as a muon identifier it is necessary to measure the probability  $\epsilon_p$  that hadrons penetrate the  $\mu_1$  absorber. A sample of events with muons identified by the counter configuration  $\bar{A}EBC$  were used to measure the penetration (punch-through) probability of the accompanying hadrons as a function of the  $z$  position of the event vertex [Fig. 3(a)], and as a function of the energy of the hadronic shower [Fig. 3(b)]. The shapes of these dependences are consistent with other measurements<sup>8</sup> of hadron penetration as indicated in Figs. 3(a) and 3(b).

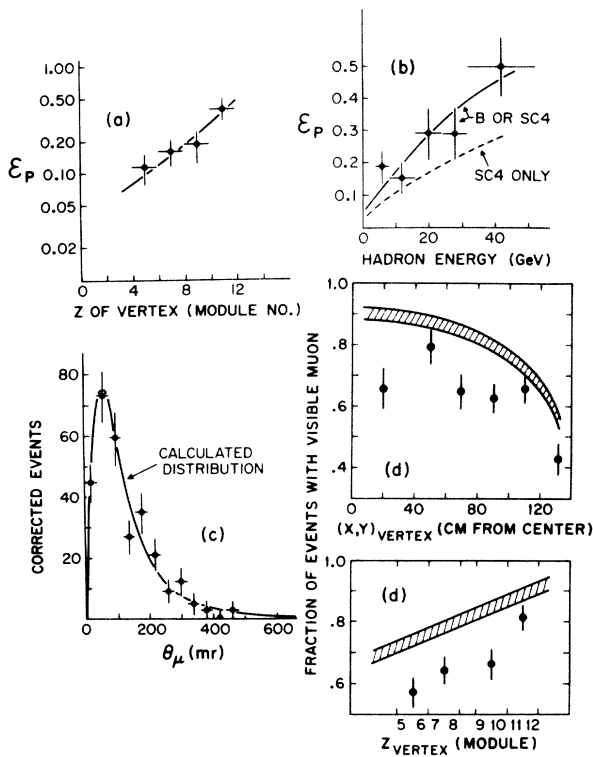


FIG. 3. (a) The measured punch-through probability of hadrons accompanying  $\bar{A}EBC$  events (for all hadron energies) as a function of  $z$ , and the expected shape of the distribution. (b) The measured punch-through probability (for  $z$  between 5 and 12) as a function of  $E_H$ , compared with the expected variation. (c) The corrected muon angular distribution measured in SC4 compared with the predicted distribution. (d) Comparison of the observed fraction of events with a muon for the  $\mu_1'$  identifier (SC4 alone) and  $\epsilon_\mu$  as functions of transverse position and  $z$  position. The cross-hatching indicates the uncertainty in  $\epsilon_\mu$  arising from the statistics of the data in (c).

The angular distribution of muons<sup>9</sup> identified by a spark in SC4 (for about  $\frac{2}{3}$  of the muon sample) is shown as the histogram in Fig. 3(c), after correction for the geometric acceptance of SC4. The geometric acceptance of SC4 is calculated using only the observed distributions of event vertex positions and assuming azimuthal symmetry of the primary neutrino interaction. The raw data divided by the calculated acceptance yield directly the intrinsic muon angular distribution in Fig. 3(c). Calculations which use the measured neutrino-antineutrino spectrum and a model of the interaction dynamics<sup>4</sup> yield the intrinsic muon angular distribution shown by the solid curve in Fig. 3(c). We conclude from the good agreement in Fig. 3(c) that these latter calcula-

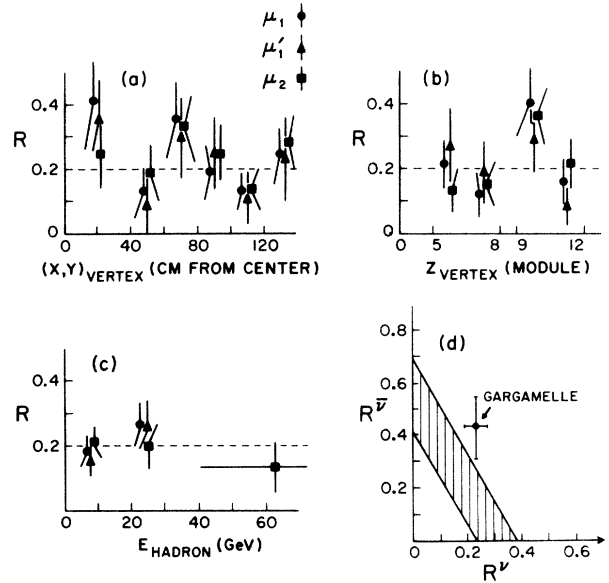


FIG. 4. (a)  $R$  obtained from three different muon identifiers as a function of the transverse distance from the center of the calorimeter. (b) The  $z$  variation of  $R$  obtained using three different muon identifiers. (c) The  $E_H$  variation of  $R$  from three muon identifiers. (d) The allowed region of  $R^\nu$  and  $R^{\bar{\nu}}$  from this experiment compared with  $R^\nu$  and  $R^{\bar{\nu}}$  obtained in the CERN measurement (Ref. 2).

tions reproduce the observed angular distribution out to the maximum detected angle of 500 mrad. Only 4% of the muons are predicted to lie at angles greater than 500 mrad. The muon detection efficiency  $\epsilon_\mu$  is then obtained from the measured angular distribution, corrected for the loss of events with  $\theta_\mu > 500$  mrad.<sup>10</sup>

The ratio of muonless events to events with muons is obtained from the formula

$$R = \frac{[\epsilon_\mu + \epsilon_p - \epsilon_\mu \epsilon_p](1 + R_m) - 1}{1 - \epsilon_p(1 + R_m)}, \quad (1)$$

where  $R_m$  is the measured ratio of events without and with a count in a given muon identifier. In Fig. 3(d) we plot the observed fraction of events with a muon as a function of  $z$  and of  $(x, y)$ , after correction for hadron punch-through, which should be equal to  $\epsilon_\mu$  if  $R=0$  [Eq. (1)]. The data were obtained using SC4 alone as a muon identifier ( $\mu_1'$ ), and are to be compared with  $\epsilon_\mu$ , shown as the cross-hatched regions in Fig. 3(d). A clear discrepancy is indicated, providing evidence that  $R$  is different from zero.

Figures 4(a), 4(b), and 4(c) present  $R$  as a function of (a) the transverse position of the event vertex, (b) the  $z$  position of the event ver-

tex, and (c) the hadron energy  $E_H$ . We have included in Fig. 4 results for SC4 alone ( $\mu_1'$ ), as well as for  $\mu_1$  and  $\mu_2$ . The best solid angle is achieved with  $\mu_1$ , but for  $\mu_1'$  the measured values of  $\epsilon_p$  are smaller than for  $\mu_1$  [Fig. 3(b)], and for  $\mu_2$ ,  $\epsilon_p=0$ . Furthermore, the dependence on  $z$ ,  $(x, y)$ , and  $E_H$  of the  $\epsilon_\mu$  for  $\mu_1$ ,  $\mu_1'$ , and  $\mu_2$  is significantly different, which serves to test the internal consistency of the data.<sup>11</sup> Apart from statistical fluctuations, Fig. 4 indicates that the same value of  $R$  is obtained from each of the muon identifiers over the entire range of each of the variables plotted and provides evidence for stability of the results. These results integrated over  $z$ , transverse position, and  $E_H$  yield

$$R = 0.20 \pm 0.05,$$

where the error includes an estimate of 0.03 for possible systematic effects, which follows from an exhaustive study of the sensitivity of  $R$  to changes in the measured variables.

The value of  $R$  measured for the combined neutrino-antineutrino beam used in this experiment is related to the values of  $R^\nu$  and  $R^{\bar{\nu}}$ , for pure neutrinos and antineutrinos, respectively, by

$$R = aR^\nu + (1-a)R^{\bar{\nu}},$$

where  $a = 0.63 \pm 0.11$  is the corrected observed ratio of the negative muon event rate to the total muon event rate. The allowed values of  $R^\nu$  and  $R^{\bar{\nu}}$  are presented in Fig. 4(d) which also shows the recent results for  $R^\nu$  and  $R^{\bar{\nu}}$  from Gargamelle.<sup>2</sup>

It is a pleasure to acknowledge the aid and encouragement of the National Accelerator Labora-

tory staff and the efforts of Robert Beck and Hans Weeden.

\*Work supported in part by the U. S. Atomic Energy Commission under Contract No. AT(11-1)-881-401.

†On leave of absence from Laboratoire de L'Accélérateur Lineaire, Orsay, France.

‡Now at Stanford Linear Accelerator Center, Stanford, Calif. 94305.

§Alfred P. Sloan Foundation Fellow, now at the University of Chicago, Chicago, Ill. 60637

<sup>1</sup>A. Benvenuti *et al.*, Phys. Rev. Lett. **32**, 1025 (1974).

<sup>2</sup>F. J. Hasert *et al.*, Phys. Lett. **46B**, 138 (1973), and CERN Report No. TC-L/Int. 74-1 (to be published).

<sup>3</sup>The horn was constructed under the supervision of F. Nezrick.

<sup>4</sup>A. Benvenuti *et al.*, Phys. Rev. Lett. **30**, 1084 (1973), and **32**, 125 (1974).

<sup>5</sup>The triggering circuitry was determined from the data to be fully efficient for hadron energy  $E_H > 4$  GeV.

<sup>6</sup>For  $\overline{AEB}$  triggers the ratio of verticized events to all events is 0.22 for  $E_H < 12$  GeV and 0.57 for  $E_H > 12$  GeV, for  $\overline{AEB}$  events the corresponding ratios are 0.57 and 0.74.

<sup>7</sup>As Fig. 3(d) shows, the data do not indicate any excess of muonless events near the edges (142 cm) of the detector.

<sup>8</sup>R. W. Ellsworth *et al.*, Phys. Rev. **165**, 1449 (1968).

<sup>9</sup>The angle of the muon is determined from the angle of the 10-cm-long track segment in SC4 and from the line joining the track centroid to the shower vertex.

<sup>10</sup>The detection efficiency  $\epsilon_\mu$  includes a small correction ( $\sim 0.3\%$ ) for muons within the angular acceptance that range out.

<sup>11</sup>For muon identifiers  $\mu_1$ ,  $\mu_1'$ , and  $\mu_2$  the average  $\epsilon_\mu$  are 0.89, 0.81, and 0.79.

## Measurement of Rates for Muonless Deep Inelastic Neutrino and Antineutrino Interactions\*

B. Aubert,† A. Benvenuti, D. Cline, W. T. Ford, R. Imlay, T. Y. Ling, A. K. Mann, F. Messing, J. Pilcher,‡ D. D. Reeder, C. Rubbia, R. Stefanski, and L. Sulak  
*Department of Physics, Harvard University, Cambridge, Massachusetts 02138, and*  
*Department of Physics, University of Pennsylvania, Philadelphia, Pennsylvania 19174, and*  
*Department of Physics, University of Wisconsin, Madison, Wisconsin 53706, and*  
*National Accelerator Laboratory, Batavia, Illinois 60510*

(Received 16 May 1974)

Relative rates for deep inelastic neutrino and antineutrino scattering without a final-state muon have been measured. For neutrinos the result is  $R^\nu = \sigma(\nu_\mu + \text{nucleon} \rightarrow \nu_\mu + \text{hadrons}) / \sigma(\nu_\mu + \text{nucleon} \rightarrow \mu^- + \text{hadrons}) = 0.11 \pm 0.05$ . The corresponding ratio for antineutrinos is  $R^{\bar{\nu}} = 0.32 \pm 0.09$ .

We have reported previously<sup>1,2</sup> the observation of deep inelastic neutrino and antineutrino interactions in which no muon appeared in the final

state. In those experiments a value of  $R$ , the ratio of the number of events without to the number of events with a muon, was obtained utilizing